ACS APPLIED MATERIALS & INTERFACES

Research Article

www.acsami.org

In Situ Control of Underwater-Pinning of Organic Droplets on a Surfactant-Doped Conjugated Polymer Surface

Wei Xu, Jian Xu, Chang-Hwan Choi, and Eui-Hyeok Yang*

Department of Mechanical Engineering, Stevens Institute of Technology, Hoboken, New Jersey 07030, United States

Supporting Information

ABSTRACT: Controlling the pinning of organic droplets on solid surfaces is of fundamental and practical interest in the field of material science and engineering, which has numerous applications such as surface cleaning, water treatment, and microfluidics. Here, a rapid in situ control of pinning and actuation of organic droplets is demonstrated on dodecylbenzenesulfonate-doped polypyrrole (PPy(DBS)) surfaces in an aqueous environment via an electrochemical redox process. A dramatic change of the pinning results from the transport of DBS^- molecules between the PPy(DBS) surface and the aqueous environment, as well as from a simultaneous alternation of the surface oleophobicity to organic liquids during the redox process. This in situ control of the droplet pinning enables a stop-and-go droplet actuation, applicable to both polar and apolar organic droplets, at low voltages (~0.9 V) with an extremely low roll-off angle (~0.4°).

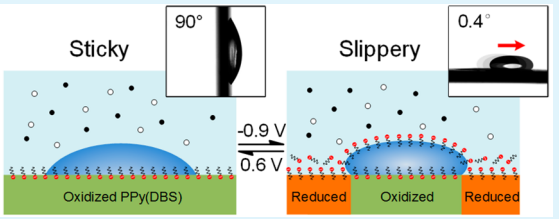

KEYWORDS: *pinning, actuation, droplets, surfactants, polypyrrole*

1. INTRODUCTION

Surfaces found in nature exhibit various liquid affinities that enable their specific functions. For instance, lotus leaves show an ultralow resistance to water droplets so that they easily roll off the leaves and spontaneously remove debris from the surface.[1] Similar to the lotus, certain species of fish are covered with superoleophobic scales that repel oil contaminants found in water.[2] In contrast to these examples, surfaces found on the petal of a rose exhibit a strong pinning effect when in contact with liquids.[3] Inspired by nature, researchers have designed and fabricated various artificial surfaces with desirable droplet pinning for a wide range of applications, including self-cleaning,[1,4−6] frictional drag reduction,[7−11] antifouling,[12−14] antifrosting/icing,[15−17] and droplet manipulation.[18−21] Nowadays, surfaces with controllable droplet pinning have gained a great deal of attention for their applications in microfluidics, lab-on-chip devices, sensors, and water treatments.[22−28] Researchers have developed various methods to manipulate the pinning of liquid droplets on surfaces via the application of external stimuli such as light,[29] heat,[30] electrical potential,[31] magnetic field,[32] and mechanical stress,[33] as well as through the modulation of the pH[34] or surfactant concentration[35] of the surrounding liquid medium. According to the Furmidge equation,[36] the pinning force of a moving droplet on an inclined surface is represented as

$$mg \sin \alpha = w\gamma(\cos \theta_R - \cos \theta_A) \quad (1)$$

where m is the mass of the droplet, g is the constant of gravitational acceleration, α is the roll-off angle, w is the width of the droplet, γ is the interfacial tension between the droplet and the surrounding medium, and θ_R and θ_A are the receding and advancing contact angles of the droplet. It reveals that both the interfacial tension (γ) of a liquid droplet and the contact angle hysteresis ($\theta_R - \theta_A$) affect the droplet pinning force on a surface. However, existing approaches report the control of droplet pinning by merely changing the wetting property of a substrate (i.e., contact angle and contact angle hysteresis resulting from the change of the interfacial tension of a solid substrate with the surrounding medium),[29−35] for instance, from hydrophobic (oleophilic) to hydrophilic (oleophobic) or vice versa but not the interfacial tension of a droplet with the surrounding medium.

Here, we show a novel mechanism of achieving an in situ control of the underwater-pinning of organic droplets using the electrochemical redox process of dodecylbenzenesulfonate-doped polypyrrole (PPy(DBS)) surfaces, enabled by a simultaneous modulation of (1) the interfacial tension at the solid−aqueous medium interface and (2) the interfacial tension at the droplet−aqueous medium interface. We show that during the reduction of the polymer, the interfacial tension of a droplet with the surrounding medium decreases due to a release of DBS^- molecules from PPy(DBS), and the contact angle increases due to an oleophobic tuning of the surface. Conversely, we demonstrate that the interfacial tension increases and the contact angle decreases during oxidation as a consequence of the recombination of DBS^- molecules with the PPy(DBS) surface, in addition to the oleophilic tuning of the surface. We furthermore show that the conversion between reduction and oxidation enables an in situ control of the pinning of organic droplets on a PPy(DBS) surface in an

Received: March 31, 2015
Accepted: November 4, 2015

DOI: 10.1021/acsami.5b07589
ACS Appl. Mater. Interfaces XXXX, XXX, XXX−XXX

aqueous environment, demonstrating an extremely low roll-off angle. Finally, we show that the control of the pinning on PPy(DBS) surfaces is applicable to both polar and apolar organic droplets.

2. EXPERIMENTAL SECTION

Synthesis and Redox of PPy(DBS). PPy(DBS) surfaces were fabricated via electropolymerization on a Cr/Au-coated silicon substrate. The Cr (30 nm) and Au (30 nm) coatings were deposited on the silicon substrate using an e-beam evaporator (Explorer 14, Denton Vacuum, Moorestown, NJ, USA). The PPy(DBS) films were then electropolymerized on the Cr/Au-coated silicon substrate. During the electropolymerization, the substrate was submerged in a solution consisting of 0.1 M pyrrole (reagent grade, 98%, Sigma-Aldrich, St. Louis, MO, USA) and 0.1 M sodium dodecylbenzenesulfonate (NaDBS) (technical grade, Sigma-Aldrich, St. Louis, MO, USA) as the working electrode. A saturated calomel electrode (SCE) (Fisher Scientific Inc., Pittsburgh, PA, USA) and a Cr/Au-coated silicon wafer were also submerged in the solution as the reference electrode and the counter electrode. The deposition of PPy(DBS) on the Cr/Au-coated silicon substrate was carried out at 0.8 V versus SCE by setting the surface charge density to 300 mC·cm^{-2}, using a potentiostat (263A, Princeton Applied Research, Oak Ridge, TN, USA).[37] The applied surface charge density controlled the thickness of the PPy(DBS) coating. The PPy(DBS) layer coated with a surface charge density of 300 mC·cm^{-2} was ~1.6 μm thick. The substrate with the PPy(DBS) coating was then cleaned by rinsing with deionized (DI) water. The surface morphology of the PPy(DBS) coating was characterized via scanning electron microscope (Auriga small dual-beam FIB-SEM, Carl Zeiss, Jena, Germany) and atomic force microscope (Nano-I AFM, Pacific Nanotechnology, Santa Clara, CA, USA). The reduction/oxidation of PPy(DBS) was conducted in a three-electrode system in 0.1 M $NaNO_3$ (≥99.0%, Sigma-Aldrich, St. Louis, MO, USA) solution using constant voltages (263A, Princeton Applied Research, Oak Ridge, TN, USA). During the reduction/oxidation, the PPy(DBS)-coated substrate, a platinum mesh (13 mm × 35 mm), and an SCE were used as the working electrode, counter electrode, and reference electrode, respectively. A voltage of −0.9 V was applied to the PPy(DBS)-coated substrate for the reduction of PPy(DBS) and a voltage of 0.6 V was used for the oxidation, which were chosen according to the cyclic voltammogram of the reduction−oxidation reaction of PPy(DBS).[37] The PPy films without DBS^- doped were synthesized in 0.1 M pyrrole solution at 0.8 V versus SCE with a surface charge density of 300 mC·cm^{-2} and tested as control samples. All solutions were prepared with DI water (>1 MΩ·cm, Milli-DI system, EMD Millipore, Billerica, MA, USA).

Characterization of Droplet Pinning. The pinning of organic droplets on PPy(DBS) surfaces was characterized according to the roll-off angles of organic droplets in 0.1 M $NaNO_3$ solution on top of the PPy(DBS) surfaces in both reduced and oxidized states using a goniometer system (model 500, Ramé-hart, Netcong, NJ, USA). The configuration of the experimental setup is shown in Figure S1 in Supporting Information. The PPy(DBS) samples were tested in a quartz cell (45 mm × 30 mm × 45 mm deep) filled with 0.1 M $NaNO_3$. The counter electrode was a 13 mm × 35 mm platinum mesh, which was vertically placed in the $NaNO_3$ solution at a corner of the quartz cell. An SCE was used as the reference electrode, which was placed in the center of the cell. The contact angle and the profile of organic droplets were also monitored using the goniometer system. Dichloromethane (DCM, ≥99.8%, Sigma-Aldrich, St. Louis, MO, USA), hexane (anhydrous, 95%, Sigma-Aldrich, St. Louis, MO, USA), and octane (anhydrous, ≥99%, Sigma-Aldrich, St. Louis, MO, USA) droplets were tested as the organic droplets.

Release of Surfactants. The release of DBS^- molecules from PPy(DBS) into the aqueous environment was investigated by two methods. First, the energy dispersive X-ray spectroscopy (EDS) (Auriga small dual-beam FIB-SEM, Carl Zeiss, Jena, Germany) was used to measure the content change of sulfur (S) in the PPy(DBS) surface during reduction, oxidation, and the cycles of redox, respectively. The content (atom %) of sulfur during reduction (−0.9 V) and oxidation (0.6 V) was measured at 0, 5, 10, 50, 100, 500, and 1000 s. The content (atom %) of sulfur was also measured after 0, 1, 2, 5, 10, 20, and 50 redox cycles. In each cycle, the reduction was conducted at a voltage of −0.9 V for 15 s and the oxidation was achieved at a voltage of 0.6 V for 15 s. The beam energy was 5 kV, and the analyzed area was ~74 μm^2. Second, a DCM droplet was placed at a distance of 0.2 mm near a PPy(DBS) surface, which had been reduced at a voltage of −0.9 V for 100 s. The change of shape of the DCM droplet was monitored and used to calculate the change of interfacial tension of the DCM droplet.

Droplet Manipulation. The transportation of a DCM droplet on a PPy(DBS) surface was monitored using the goniometer system (model 500, Ramé-hart, Netcong, NJ, USA). The PPy(DBS) surface was tilted to 1.5°. Initially an oxidative potential (0.6 V) was applied on the PPy(DBS) substrate. Then, the DCM droplet was dispensed on the PPy(DBS) in a 0.1 M $NaNO_3$ aqueous environment using a dispensing syringe (~1 μL). The working electrode potential was adjusted in cycles of −0.9 V for 8 s and 0.6 V for 10 s using a potentiostat (263A, Princeton Applied Research, Oak Ridge, TN, USA). The shape and the contact angle of the DCM droplet upon the repetitive PPy(DBS) redox cycles were monitored and recorded.

3. RESULTS AND DISCUSSION

Figure 1 illustrates the proposed mechanism and a representative droplet behavior, showing an in situ control of the pinning of a DCM droplet on an electropolymerized PPy(DBS) surface (the surface morphology is shown in Figure S2, Supporting Information) in an aqueous electrolyte

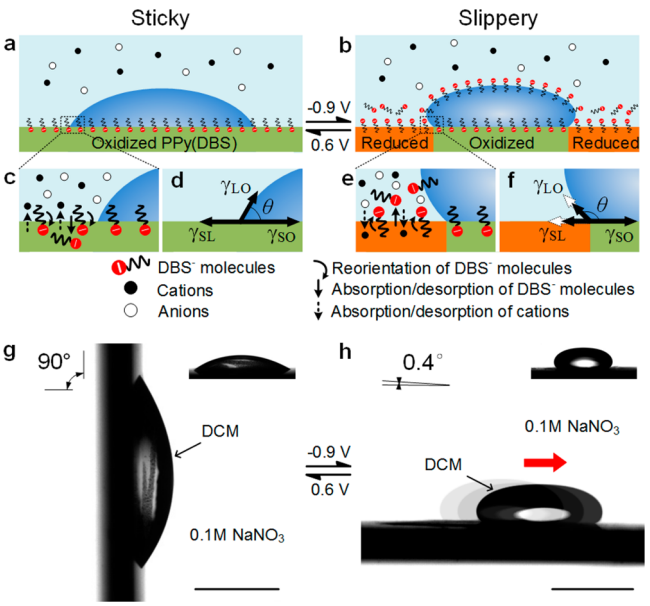

Figure 1. In situ control of the pinning of an organic droplet on a PPy(DBS) surface. (a, c, d) At a voltage of 0.6 V, the PPy(DBS) surface is oxidized and observably sticky to organic droplets. (b, e, f) At a voltage of −0.9 V, the PPy(DBS) surface becomes slippery to organic droplets due to a dramatic decrease of pinning force; this decrease is caused by the simultaneous alternation of the surface oleophobicity and the decrease of interfacial tension at the droplet−aqueous medium interface, which are induced by the reorientation and the desorption of surfactant (DBS^-) molecules from PPy(DBS) during the reduction, respectively. (g, h) The in situ control of the pinning of dichloromethane (DCM) droplets on a PPy(DBS) surface in 0.1 M $NaNO_3$ solution. γ_{SL}, γ_{SO}, and γ_{LO} are the interfacial tensions at the interfaces of PPy(DBS)−aqueous medium, PPy(DBS)−droplet, and droplet−aqueous medium, respectively. Scale bars = 1 mm.

DOI: 10.1021/acsami.5b07589
ACS Appl. Mater. Interfaces XXXX, XXX, XXX−XXX

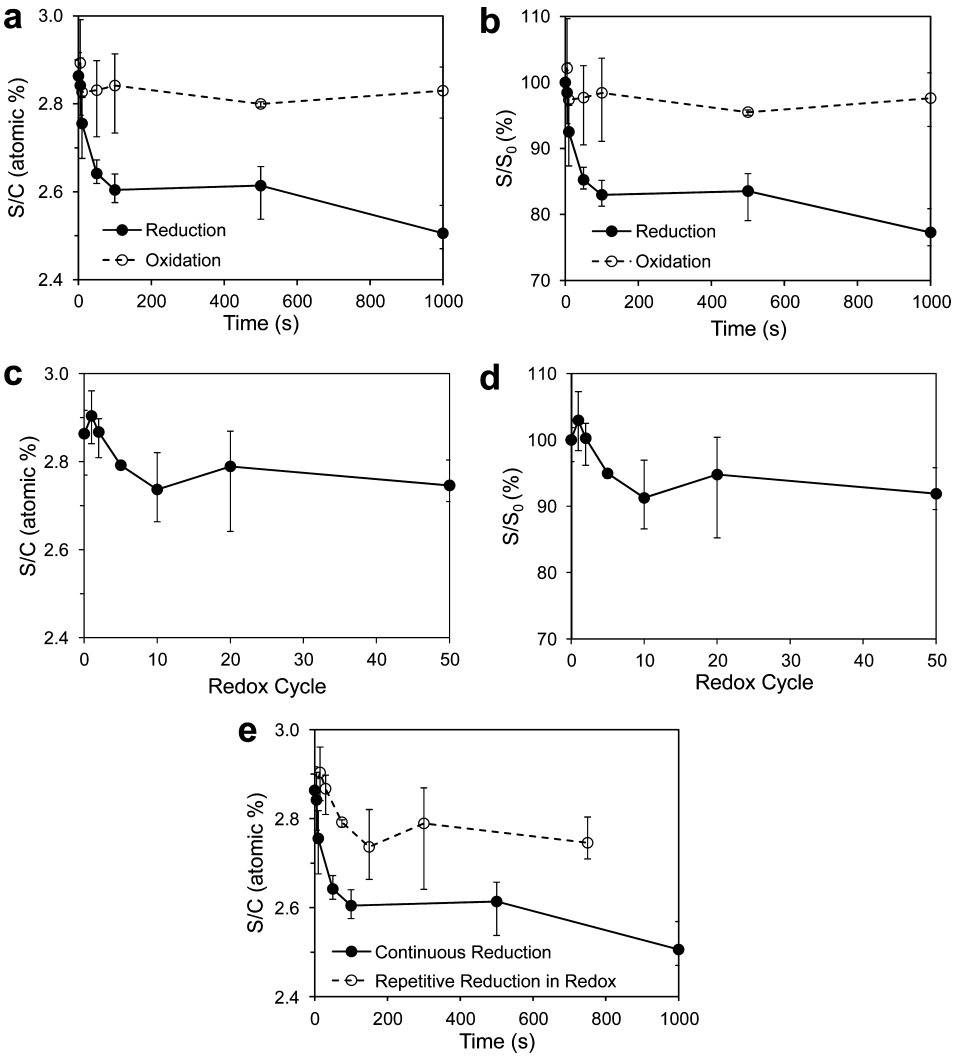

Figure 2. Release of DBS^- molecules from PPy(DBS). (a, b) Change in the atomic ratio of sulfur (S) to carbon (C) in the PPy(DBS) coating (S/C) and the rate of change of the sulfur content remaining in the PPy(DBS) with respect to the initial state (S/S_0) during continuous reduction and oxidation mode, respectively. (c, d) Change in atomic ratio of sulfur (S) to carbon (C) in the PPy(DBS) coating (S/C) and the rate of change of the sulfur content remaining in the PPy(DBS) with respect to the initial state (S/S_0) during repetitive redox cycles (reduction for 15 s and then oxidation for 15 s per cycle), respectively. (e) Comparison of the change in atomic ratio of sulfur (S) to carbon (C) in the PPy(DBS) coating (S/C) during continuous reduction and that in repetitive reduction through redox cycles.

environment (0.1 M $NaNO_3$ solution) via a low-voltage (<1 V) redox process. In an oxidized state, upon the application of a voltage of 0.6 V (Figure 1a), the DBS^- surfactant molecules bond to the PPy chains via ionic bonding with polar sulfonic acid groups, allowing the dodecyl chains to protrude out from the polymer chains and constitute the surface layer. Since the strongly hydrophilic (or oleophobic) polar sulfonic acid groups are attracted to the polymer backbone and the hydrophobic (or oleophilic) dodecyl groups situate to the external surface, the oxidized PPy(DBS) surface exhibits a state of underwater oleophilicity and strong pinning to organic droplets. For example, the apparent contact angle of a DCM droplet is ~32° on the oxidized PPy(DBS) surface (the inset of Figure 1g) and the droplet is strongly pinned on the surface; thus, it does not move at all, even when the surface is tilted vertically (Figure 1g).

Upon the application of a voltage of −0.9 V (Figure 1b), the PPy(DBS) surface exposed to the aqueous electrolyte is reduced and absorbs cations from the electrolyte for charge neutralization (Figure 1e).[37] However, the surface area underneath the droplet still remains oxidized due to the absence of cations. The DBS^- molecules in the reduced PPy(DBS) no longer bond to PPy backbones; rather they reorient within the PPy(DBS), exposing the hydrophilic (or oleophobic) sulfonic acid groups at the outermost surface. This change makes the reduced polymer surface hydrophilic (or oleophobic) and consequently decreases the interfacial tension at the PPy(DBS)−aqueous medium interface (γ_{SL}, Figure 1f). As a consequence of the decreased γ_{SL}, the contact angle of the droplet increases according to the Young's equation, which is represented as

$$\cos\theta = \frac{\gamma_{SL} - \gamma_{SO}}{\gamma_{LO}} \quad (2)$$

where θ is the contact angle of a droplet, and γ_{SL}, γ_{SO}, and γ_{LO} are the interfacial tensions at the interfaces of PPy(DBS)−aqueous medium, PPy(DBS)−droplet, and droplet−aqueous medium, respectively. In addition, although the majority of the DBS^- molecules are locked in the PPy(DBS) matrix due to the

DOI: 10.1021/acsami.5b07589
ACS Appl. Mater. Interfaces XXXX, XXX, XXX−XXX

bulkiness of volume,[38−40] a minute amount of DBS^- molecules can escape from the PPy(DBS) surface during reduction and accumulate at the interface between the organic droplet and the aqueous medium (Figure 1e). This results in a significant decrease of the interfacial tension at the droplet−aqueous medium interface during the reduction (γ_{LO}), as indicated by the flattening of the organic droplet on the reduced PPy(DBS) substrate (the inset of Figure 1h). Once the contact angle increases greater than 90° with the decrease of the interfacial tension at the PPy(DBS)−aqueous medium interface (γ_{SL}), the decrease of the interfacial tension at the droplet−aqueous medium interface (γ_{LO}) further amplifies the change of the contact angle according to eq 2. As shown in the inset of Figure 1h, the contact angle of a DCM droplet apparently increases to 140° upon reduction. Furthermore, the pinning force of the organic droplet is also significantly decreased with the decrease of the interfacial tension at the droplet−aqueous medium interface and the increase of the surface oleophobicity according to the Furmidge equation (eq 1) so that the droplet becomes more mobile with less friction during movement. On a stage with a tilting angle as low as 0.4°, the droplet slides off from the reduced surface, showing the high slipperiness of the surface (Figure 1h). The PPy(DBS) surface switches back to the sticky state under oxidation via the reorientation/absorption of DBS^- molecules and the desorption of cations out of the PPy(DBS) film (Figure 1c). Thus, the low-voltage redox process of the PPy(DBS) surface enables an in situ control of the underwater-pinning (i.e., from sticky to slippery and vice versa) of organic droplets.

We used EDS analysis to examine the release of DBS^- molecules from the PPy(DBS) surface during the redox process (described in detail in the Experimental Section). Although the DBS^- molecules in PPy(DBS) are reportedly retained in the polymer during the redox and the electroneutrality is preserved by the diffusion of cations according to a previous qualitative study using probe beam deflection and quartz crystal microbalance techniques,[39,40] our quantitative EDS analysis shows that DBS^- molecules are gradually released from the polymer matrix during the redox. As shown in Figure 2a, the average atomic ratio of sulfur (S) to carbon (C) was approximately 2.86% in the as-deposited PPy(DBS) samples, which practically agrees with the ratio of S/C calculated according to the chemical composition of PPy(DBS) (2.94%). However, the ratio of S/C in PPy(DBS) films gradually decreased to 2.76%, 2.60%, and 2.51% after a reduction for 10, 100, and 1000 s, respectively, while there was no significant change in the ratio of S/C during oxidation. Since the sulfur (S) in PPy(DBS) only exists in DBS^- molecules, the content decrease of sulfur confirms that DBS^- molecules were released from PPy(DBS) films during the redox process, particularly during reduction. Figure 2b further shows the change of sulfur (S) in PPy(DBS) in regard to the initial state (S_0). The ratio of sulfur to the initial state (S/S_0) gradually decreased during the reduction. After 1000 s of reduction, only 77% of the initial sulfur (i.e., DBS^- molecules) was retained in the PPy(DBS). During the repetitive redox cycles (reduction for 15 s and then oxidation for 15 s in each redox cycle), the ratio of S/C in PPy(DBS) films also gradually decreased to 2.79% and 2.74% after 5 and 50 redox cycles, respectively (Figure 2c). After 50 redox cycles, the content of sulfur (i.e., DBS^- molecules) in the PPy(DBS) decreased to 91% of the initial state (Figure 2d). Compared to the decreasing rate of the content of sulfur during continuous reduction, the release rate of DBS^- during the repetitive redox cycle was slower as shown in Figure 2e (e.g., the redox cycles of 1, 10, and 50 correspond to 15, 150, and 750 s for the total reduction time). This implies that some of DBS^- molecules, which had been released from PPy(DBS) during the reduction process of the redox cycles, reentered into the PPy(DBS) during the oxidation process and consequently slowed down the release rate of the DBS^- molecules.

To prove that the DBS^- molecules released from the PPy(DBS) surface accumulate at the interface between the droplet and the aqueous medium, we examined the change in the shape of a pendent DCM droplet located near the PPy(DBS) surface immersed in the aqueous medium. In this test, a PPy(DBS) surface was first reduced for 100 s and then a pendent DCM droplet (~1 mm in diameter) was placed near the reduced PPy(DBS) surface at a distance of 0.2 mm (Figure 3a). The DCM droplet near the reduced PPy(DBS) surface

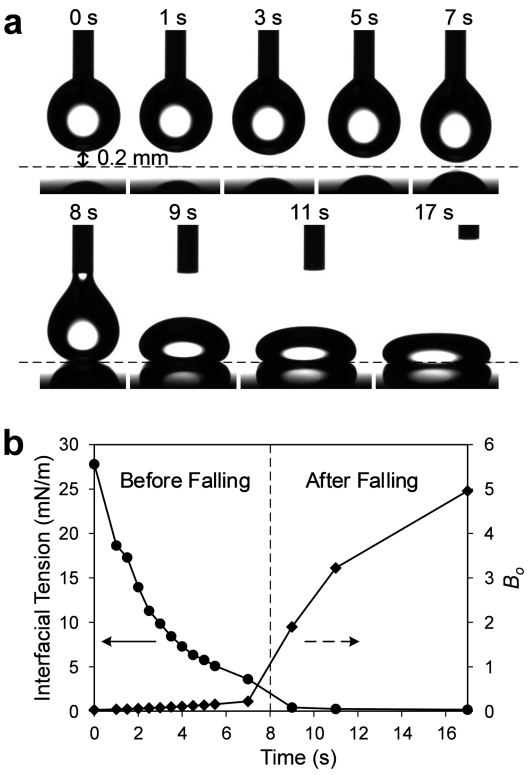

Figure 3. (a) Shape change and falling process of a DCM droplet, placed at 0.2 mm away from a reduced PPy(DBS) substrate. The dashed line indicates the location of a substrate surface. Spherical-cap-like objects below the dashed line are the reflections of the droplet from the PPy(DBS) surface. (b) Change of interfacial tension and Bond number (B_o) during the falling process.

gradually changed from a spherical shape to a spindle in approximately 7 s and then fell down from the needle, landing on the PPy(DBS) surface at approximately 8 s. The initial shape of the pendent droplet is retained by the equilibrium between capillary force and gravity. Therefore, the shape change and the fall of the droplet indicate a decrease in capillary force, induced by the decrease of interfacial tension at the droplet−aqueous medium interface. Since the DBS^- molecules (surfactants) in the aqueous medium decrease the interfacial tension of a pendent DCM droplet with the surrounding aqueous medium (Figure S3, Supporting Information), this result provides further evidence of the release of DBS^- molecules from PPy(DBS) and their accumulation around

DOI: 10.1021/acsami.5b07589
ACS Appl. Mater. Interfaces XXXX, XXX, XXX−XXX

the droplet−aqueous medium interface. Figure 3b shows the change in the interfacial tension of a DCM droplet during the falling process. The interfacial tension of the pendent droplet before the fall was measured using a goniometer, based on the Young−Laplace equation.[41,42] The interfacial tension after the fall was calculated based on a balance between the Laplace pressure and the hydrostatic pressure of the droplet according to the flattened droplet shape (Figure S4, Supporting Information). The interfacial tension was significantly decreased from 27.8 to 3.6 mN·m^{-1} in approximately 7 s before the droplet fell onto the PPy(DBS) surface. Once the DCM droplet landed on the PPy(DBS) surface, it was flattened as shown in Figure 3a. Here, the interfacial tension was further decreased to 0.16 mN·m^{-1} due to additional accumulation of the released and unconstrained DBS$^-$ molecules on the surface of the DCM droplet. To estimate the time scale of the desorption process of DBS$^-$ from PPy(DBS) and the subsequent adsorption on a droplet, a pendent DCM droplet (0.8 μL) in 0.1 M $NaNO_3$, similar to Figure 3a, was placed in close proximity to the surface of an initially oxidized PPy(DBS) substrate (coated with a surface charge density of 300 mC·cm^{-2}). The gap between the droplet and the substrate was ∼0.03 mm to minimize the time for the diffusion of DBS$^-$ molecules from the PPy(DBS) surface to the droplet in the electrolyte. After a reductive voltage was applied to the PPy(DBS) substrate, the droplet changed the shape in ∼3 s and fell on the substrate. From this result, we estimate that the total time of the desorption process of DBS$^-$ from PPy(DBS) and the relaxation time of the adsorption process of DBS$^-$ on a DCM droplet was approximately 3 s (Figure S5-a, Supporting Information). We also found that a pendent DCM droplet in 0.1 M $NaNO_3$ deformed and detached in ∼0.2 s when it was contacted with a small amount of NaDBS solution (0.001 M) (Figure S5-b, Supporting Information). This indicates that the relaxation time of the adsorption process is quite shorter than the response time of shape change of the DCM droplet on the PPy(DBS) surface. Therefore, the desorption process of DBS$^-$ from PPy(DBS) is primarily responsible for determining the response time of shape change of the DCM droplet, and the time scale of the adsorption process of DBS$^-$ to the droplet−aqueous medium interface is negligible in the actuation mechanism.

The significant decrease of the interfacial tension at the droplet−aqueous medium interface has two implications. First of all, the droplet flattens with a significantly decreased interfacial tension. Figure 3b shows the change of the Bond number (B_o) resulting from the decrease of interfacial tension during the fall of a droplet. The B_o number is the ratio of the gravitational and interfacial tension forces, defined by

$$B_o = \frac{\Delta\rho g R^2}{\gamma} \tag{3}$$

where $\Delta\rho$ is the difference in density between the droplet and the surrounding medium, g is the constant of gravitational acceleration, R is the characteristic length (e.g., the radius of the droplet), and γ is the interfacial tension of the droplet with the surrounding medium (i.e., γ_{LO}).[43] A low B_o number (typically smaller than 1) indicates that interfacial tension dominates over gravitational body force so that the droplet would be spherical in shape. In contrast, a high B_o number (typically larger than 1) indicates that the system is more affected by gravitational force than interfacial tension, resulting in a tendency of the gravitational force to deform the spherical shape of the droplet. As shown in Figure 3b, the B_o number gradually increased, accompanied by the decrease of interfacial tension before falling, indicating an increased effect of the gravitational force on the droplet shape over time. Once the droplet falls onto the PPy(DBS) surface, the B_o number increases intensely (i.e., B_o > 1), corresponding to a significant decrease of interfacial tension, even though the DCM droplet size is ∼1 mm in diameter (the capillary length[43] of the droplet fallen on the PPy(DBS) surface was estimated to be smaller than 0.36 mm). The change of B_o number further explains the droplet flattening phenomena on a PPy(DBS) surface during reduction. The flattening of an organic droplet on conjugated polymers was previously explained from different perspectives such as the electrical double layer (EDL),[44] the Marangoni effect,[37] and the release of surfactant dopants.[45,46] In this work, we observed that apolar organics such as hexane and octane also flattened (Figure S6, Supporting Information), which cannot be explained by the EDL hypothesis.[44] In addition, as shown in Figure 3, the DCM droplet flattened on top of a uniformly reduced PPy(DBS) surface where the Marangoni effect could not be present due to the lack of surface tension gradient along the surface. In contrast, our results (Figures 2 and 3) indicate that the release of surfactant dopants (i.e., DBS$^-$ molecules) from the PPy(DBS) surface during reduction plays a major role in the flattening of an organic droplet on surfactant-doped conjugated polymers. Second, according to the Furmidge equation (eq 1),[36] a significantly decreased interfacial tension at the droplet−aqueous medium interface (i.e., γ_{LO}) results in a small roll-off angle (0.4°) as shown in Figure 1d, which further confirms the effect of reduced interfacial tension on the change of the pinning state of the droplet on the reduced PPy(DBS) surface.

In Figure 4, we show the process of the contact angle change of a sessile DCM droplet on the PPy(DBS) surface, upon reduction for 15 s, from an initial 32° to 140° along with the deformation of the droplet from a spherical-cap shape to an

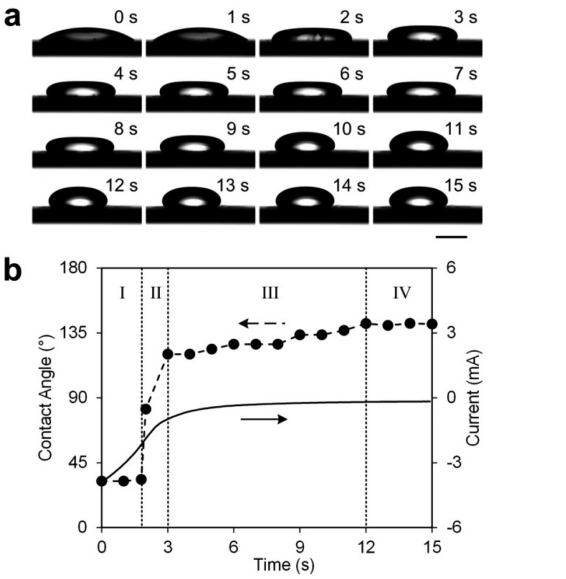

Figure 4. (a) Change of contact angle of a DCM droplet on a PPy(DBS) surface upon a reductive voltage of −0.9 V. Scale bar = 1mm. (b) The change of a contact angle can be categorized into four different stages: (I) an initial slow increase, followed by (II) a rapid increase, (III) a second slow increase, and (IV) a final stabilization.

DOI: 10.1021/acsami.5b07589
ACS Appl. Mater. Interfaces XXXX, XXX, XXX−XXX

ellipsoid as discussed in Figure 1f. On the oxidized PPy(DBS) substrate, the droplet retained the spherical-cap shape with neither flattening nor a significant increase of contact angle (Figure S7, Supporting Information). The change of a contact angle of the droplet upon reduction can be categorized in four different stages (Figure 4b): an initial slow increase (0−2 s), followed by a rapid increase (2−3 s), a second slow increase (3−12 s), and a final stabilization (12−15 s), which all relate to the reduction process of PPy(DBS). As shown in Figure 4b, the change of the chronoamperometric current after the reductive voltage application depicts the change of the charges consumed by the PPy(DBS) film,[47] indicating the occurrence of the electrochemical reaction of the PPy(DBS). The change of current was intense at the beginning and became moderate as it approached the background current after ∼3 s, implying the completion of the reduction process of the PPy(DBS) film. Therefore, the initial slow increase of contact angle corresponds to the beginning of the reduction process of PPy(DBS), in which the surface of PPy(DBS) is not fully reduced yet. With the continued reduction of PPy(DBS) upon the voltage application (2 s), the surface property significantly changes near the droplet edge, and as a consequence, the contact angle quickly changes. After the rapid increase (3 s), the change of contact angle becomes slow again due to the moderate change of current and eventually becomes stable. The switching time of a droplet from the spherical-cap to the ellipsoidal shape was affected by the droplet volume and PPy(DBS) coating thickness. For the droplets between 0.7 and 6 μL, the switching time on PPy(DBS) surfaces coated with 300 mC·cm^{-2} surface charge density was 2−3 s, and the change was not remarkable with respect to the droplet volume. However, when the droplets were smaller than 0.2 μL, the switching time was significantly decreased to less than 0.5 s (Figure S8-a, Supporting Information). The change is due to the flattening of smaller droplets requiring less surfactants, which could be obtained in a shorter time. The thickness of PPy(DBS) coating, which was controlled by adjusting the applied surface charge density during electropolymerization, also affected the switching time of the droplet. As shown in Figure S8-b, the switching time of 1 μL droplets on the PPy(DBS) surfaces increased with the coating thickness from ∼0.4 s on ∼0.2 μm thick coating (applied surface charge density, 50 mC·cm^{-2}) to ∼2 s on ∼1.6 μm thick coating (applied surface charge density, 300 mC·cm^{-2}). We attribute this to a longer reduction process on the thicker coating according to the current change. In addition, we studied the effect of the location of the counter electrode on the switching time. The switching time of 1 μL droplets on the samples synthesized with 300 mC·cm^{-2} surface charge density was ∼2 s, and the difference was not clearly observable when the location of the counter electrode was changed in the range of 45 mm in the tested quartz cell, as shown in Figure S8-c.

The changes of contact angle and interfacial tension at the droplet−aqueous medium interface, along with the consequent droplet pinning behaviors, are repeatable with the switch of an applied voltage (by redox process). Figure 5a shows the change of contact angle of a DCM droplet on PPy(DBS) under an alternating application of voltage of −0.9 and 0.6 V. The DCM droplet on the initially oxidized PPy(DBS) surface increased in contact angle from 32° to 140° while the droplet became flattened upon reduction of the PPy(DBS) surface; the contact angle decreased back when the flattened droplet switched back to a spherical-cap shape under oxidation of the PPy(DBS) surface. The time scale for the change of contact angle and the

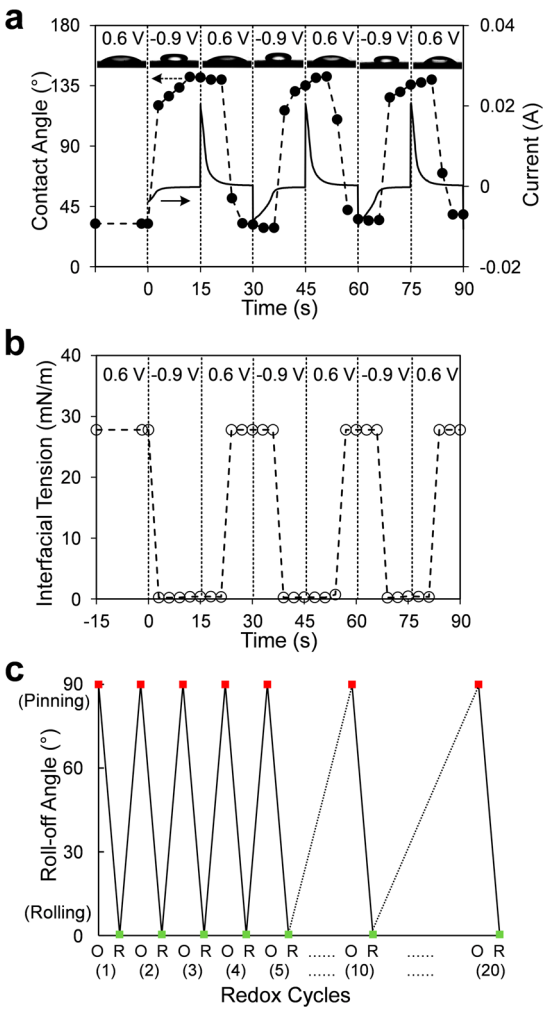

Figure 5. Control of underwater-pinning of DCM droplets on PPy(DBS) surfaces under an alternating application of voltages of −0.9 V (15 s) and 0.6 V (15 s). (a) Change of contact angle of a DCM droplet and the electric current during redox cycles. The inset shows the change of a droplet shape during the process. (b) Change of the interfacial tension of the DCM droplet on a PPy(DBS) surface during the redox process. (c) Repeatable switch of the DCM droplets between pinning states and rolling states on a PPy(DBS) surface for 20 redox cycles.

flattening of the droplet was approximately 3−6 s. This time scale agrees with the change of the electric current during the reduction and oxidation process, indicating that the change of the surface property of PPy(DBS) is directly associated with the reduction and oxidation process. We also tested DCM droplets on the PPy produced in the absence of surfactants (DBS^-) during electropolymerization. The droplets did not exhibit any change in their shapes or contact angles during the redox cycles (Figure S9, Supporting Information). This control experiment confirms the effect of surfactants on the change of droplet pinning on the PPy(DBS) surface as discussed above. It should be noted that during the multiple redox cycles, the contact angle of a DCM droplet at oxidation gradually increased (e.g., from 32° to 41° in 10 cycles). We attribute this to the change of surface roughness, the influx of water from the electrolyte into the polymer, or the accumulation of surfactant dopants on the polymer surface,[35,48−50] which affects the contact angle. Figure 5b shows the changes of interfacial tension at the droplet−aqueous medium interface of the DCM droplet on the

DOI: 10.1021/acsami.5b07589
ACS Appl. Mater. Interfaces XXXX, XXX, XXX−XXX

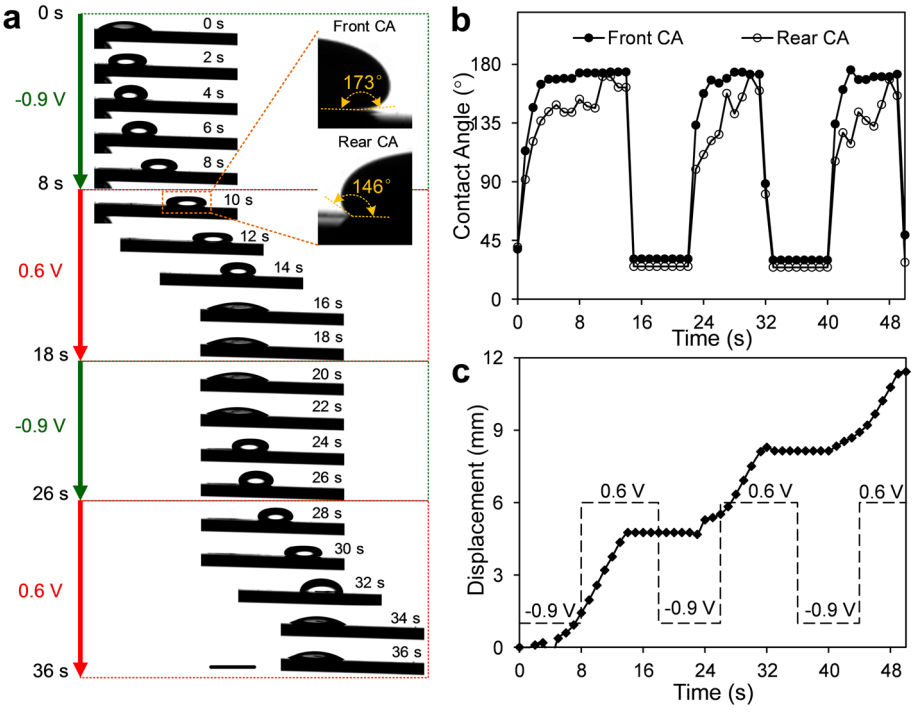

Figure 6. Controlled transportation of a DCM droplet on a PPy(DBS) surface. (a) The DCM droplet exhibited a process of successive moving and stopping on a tilted (1.5°) PPy(DBS) surface in 0.1 M $NaNO_3$, under an alternating application of voltages of −0.9 and 0.6 V. The inset shows the front advancing contact angle and the rear receding contact angle of the DCM droplet on the reduced PPy(DBS) surface during the movement, respectively. Scale bar = 2 mm. (b) Contact angles at the front and rear sides of the DCM droplet and (c) displacement of the DCM droplet during the transportation. The droplet's center before transportation was defined as the origin, and the displacement was calculated by the traveled distance of the droplet's center.

PPy(DBS) surface during the redox process. In the case of reduction, the interfacial tension of the flattened droplet was calculated according to the droplet shape using the same method employed in Figure 3 (the method is illustrated in Figure S4, Supporting Information). Since the droplet on the reoxidized PPy(DBS) surface reverted back to a spherical-cap shape (similar to the situation of the initial oxidized PPy(DBS)), the interfacial tension of the droplet at the initial state (i.e., 27.8 $mN{\cdot}m^{-1}$) was used in the case of oxidation during the redox cycles. Upon reduction, the interfacial tension at the droplet−aqueous medium interface decreased from 27.8 to 0.3 $mN{\cdot}m^{-1}$ and then increased back upon another oxidation process as shown in Figure 5b. In a test of 20 redox cycles, the DCM droplets on the PPy(DBS) surface showed a repeatable switch between a pinning state (pinned at 90° tilting angle) and a rolling state (roll-off angle, <0.4°) (Figure 5c).

We also investigated the controlled underwater-pinning of a DCM droplet on a tilted PPy(DBS) surface (coated with a surface charge density of 300 $mC{\cdot}cm^{-2}$) for a controlled droplet transportation. As shown in Figure 6a, a DCM droplet (1 μL) was initially pinned on an oxidized PPy(DBS) surface with a tilting angle of 1.5° because the pinning force overcomes the effect of gravity. The 1.5° tilting angle was chosen in order to obtain an appropriate velocity for the droplet to move within the camera's field of view as the voltage was continuously switched. Upon reduction, the DCM droplet became flattened and began to slide down the PPy(DBS) surface, since the pinning force is significantly decreased. The contact angle at a front (advancing) side of a droplet increased to 173° (Figure 6b) as it slid down the reduced PPy(DBS) surface. The contact angle at a rear (receding) side of a droplet also gradually increased to 146° in 10 s (Figure 6b). Such high contact angles indicate the underwater-superoleophobicity of the reduced PPy(DBS) surface to the DCM droplet. Here, the contact angle hysteresis is around 27°, which is relatively large in comparison to typical slippery surfaces.[4,22] However, the low interfacial tension at the droplet−aqueous medium interface (~0.3 $mN{\cdot}m^{-1}$) promotes the low roll-off angle according to the Furmidge equation (eq 1). With the movement of the droplet, the PPy(DBS) surface initially underneath the droplet is exposed to the electrolyte and further reduces with the absorption of cations from the surrounding electrolyte. Therefore, the reduction of the exposed PPy(DBS) surface follows the movement of the back edge of the droplet. Whether the reduction of the PPy(DBS) surface could catch up to the back edge of a droplet or not depends on the reduction time of the PPy(DBS) surface (~3 s according to Figure 4) and the moving velocity of the droplet. In this demonstration, the average moving velocity of the droplet was ~0.18 mm/s during the first reduction process (i.e., the first 8 s) (Figure 6c). Therefore, the reduction of the exposed PPy(DBS) surface followed the back edge of the droplet with a gap of ~0.54 mm (i.e., 0.18 mm/s × 3 s) under a reductive voltage. Upon oxidation at 8 s following the reduction, the droplet continued sliding and stopped after 6 s (i.e., at 14 s). Meanwhile, the droplet changed back to a spherical-cap shape and the contact angles of both sides dramatically decreased to less than 32°. With the continuous application of redox potentials (i.e., an alternating application of voltages of −0.9 V (8 s) and 0.6 V (10 s)), the DCM droplet exhibited a process of successive moving and stopping (Figure 6c). The switching time of ~6 s between moving and stopping is remarkably shorter than the previous report (e.g., 53 s),[49] which is attributed to the dramatic and rapid change of the pinning state of droplets on the surface.

DOI: 10.1021/acsami.5b07589
ACS Appl. Mater. Interfaces XXXX, XXX, XXX−XXX

The switching time could be further reduced on thinner PPy(DBS) coatings with smaller droplets according to the result shown in Figure S8. The pinning behavior of other organic liquids, such as hexane and octane, was also tested (Figure S10, Supporting Information). Similar to DCM droplets, they were all pinned on the oxidized PPy(DBS) surfaces, and the pinned organic droplets became flattened and then slid off the surface upon reduction of the tilted PPy(DBS) surfaces. However, the switching time for hexane and octane droplets changing from a pinning state to a rolling state was ~100 s, which was longer than that of DCM droplets, indicating a difference among organic liquids.

This work elucidates a new mechanism of an in situ control of the underwater-pinning of organic droplets on PPy(DBS) surfaces. In previous reports, the control of the pinning of liquid droplets on solid surfaces was typically achieved through ex situ processes, such as tuning the surface's chemical composition,[51] tailoring the surface morphology,[52] or applying external stimuli.[29] Whereas an in situ control of droplet pinning was also reported,[31−33] it relied on the application of a high voltage (e.g., >20 V),[31] special liquid (e.g., superparamagnetic liquids),[32] or an engineered surface.[33] In this paper, we demonstrate that an organic droplet on PPy(DBS) switches dramatically from totally pinned to extremely slippery at a low voltage (i.e., 0.9 V). Also, we demonstrate that the control of the pinning on PPy(DBS) is completed without removing liquid droplets, implying great potential for in situ manipulation of a liquid droplet. Furthermore, the control of droplet pinning is completed in a relatively short time scale (0.4−6 s), compared to previous reports on conjugated polymers (e.g., 53 s).[49] The previous approaches in literature have been only based on the change of the interfacial tension of the solid substrate with the surrounding medium. However, the demonstrated control of droplet pinning is achieved through a simultaneous modulation of the interfacial tension of the droplet with the surrounding medium, in addition to the interfacial tension of the solid substrate with the surrounding medium. The low-voltage in situ control of droplet pinning on PPy(DBS) is applicable to both polar and apolar organic droplets and therefore is a pathfinder for a broad range of applications in microfluidics, water treatments, and oil−water separation.

4. CONCLUSION

In this work, we have elucidated the mechanism for an in situ control of underwater-pinning of organic droplets on PPy(DBS) surfaces via a redox process. The control of droplet pinning on a PPy(DBS) surface has been achieved through a redox process modulated by a voltage lower than 1 V, demonstrating a dramatic conversion from sticky (upon oxidation of PPy(DBS)) to slippery (upon reduction of PPy(DBS)) or vice versa. We have also demonstrated that a reduced PPy(DBS) surface is extremely slippery to organic droplets with a roll-off angle of 0.4°. We have shown that the dramatic change in the pinning state is due to the cooperative effect of the controllable release and reorientation of surfactant dopants (i.e., DBS^- molecules), which changes the interfacial tension of the droplet with the surrounding aqueous medium and the surface wetting property, respectively, during the redox process of a PPy(DBS) surface. We have also demonstrated the controlled pinning of a DCM droplet on a tilted PPy(DBS) surface for a controllable droplet transportation. This finding on the new mechanism of the controlled underwater-pinning of organic droplets on PPy(DBS) surfaces potentially impacts several future applications including lab-on-chip technologies, water treatments, and oil−water separation.

■ ASSOCIATED CONTENT

Supporting Information

The Supporting Information is available free of charge on the ACS Publications website at DOI: 10.1021/acsami.5b07589.

Configuration of experimental setup, SEM and AFM images, interfacial tension of DCM droplets in NaDBS solutions, calculation of the interfacial tension of a flattened sessile droplet, estimation of the time of desorption of DBS^- molecules from PPy(DBS) and the adsorption on a DCM droplet, DCM droplets on oxidized PPy(DBS) surfaces and PPy surfaces without surfactant dopants, effect of droplet volume, PPy(DBS) coating thickness, position of counter electrode on the switching time, and flattening and controlled pinning of hexane and octane droplets on PPy(DBS) surfaces (PDF)

■ AUTHOR INFORMATION

Corresponding Author

*E-mail: eyang@stevens.edu.

Notes

The authors declare no competing financial interest.

■ ACKNOWLEDGMENTS

This work has been supported in part by National Science Foundation awards (Grants ECCS-1202269 and EEC-1138244) and the Defense University Research Instrumentation Program (Grant FA9550-11-1-0272). This work has also been partially carried out at the Micro Device Laboratory (MDL) and Laboratories for Multiscale Imaging (LMSI) at Stevens Institute of Technology. The authors also thank Dr. Alex Chou for his assistance on EDS characterization and Anthony Palumbo for his valuable comments.

■ REFERENCES

(1) Blossey, R. Self-Cleaning Surfaces-Virtual Realities. *Nat. Mater.* **2003**, *2*, 301−306.
(2) Liu, M.; Wang, S.; Wei, Z.; Song, Y.; Jiang, L. Bioinspired Design of a Superoleophobic and Low Adhesive Water/Solid Interface. *Adv. Mater.* **2009**, *21*, 665−669.
(3) Feng, L.; Zhang, Y.; Xi, J.; Zhu, Y.; Wang, N.; Xia, F.; Jiang, L. Petal Effect: A Superhydrophobic State with High Adhesive Force. *Langmuir* **2008**, *24*, 4114−4119.
(4) Wong, T.-S.; Kang, S. H.; Tang, S. K.; Smythe, E. J.; Hatton, B. D.; Grinthal, A.; Aizenberg, J. Bioinspired Self-Repairing Slippery Surfaces with Pressure-Stable Omniphobicity. *Nature* **2011**, *477*, 443−447.
(5) Parkin, I. P.; Palgrave, R. G. Self-Cleaning Coatings. *J. Mater. Chem.* **2005**, *15*, 1689−1695.
(6) Fürstner, R.; Barthlott, W.; Neinhuis, C.; Walzel, P. Wetting and Self-Cleaning Properties of Artificial Superhydrophobic Surfaces. *Langmuir* **2005**, *21*, 956−961.
(7) Choi, C.-H.; Kim, C.-J. Large Slip of Aqueous Liquid Flow over a Nanoengineered Superhydrophobic Surface. *Phys. Rev. Lett.* **2006**, *96*, 066001.
(8) Choi, C.-H.; Ulmanella, U.; Kim, J.; Ho, C.-M.; Kim, C.-J. Effective Slip and Friction Reduction in Nanograted Superhydrophobic Microchannels. *Phys. Fluids* **2006**, *18*, 087105−087108.
(9) Lee, C.; Choi, C.-H. Structured Surfaces for a Giant Liquid Slip. *Phys. Rev. Lett.* **2008**, *101*, 064501.

DOI: 10.1021/acsami.5b07589
ACS Appl. Mater. Interfaces XXXX, XXX, XXX−XXX

(10) Aljallis, E.; Sarshar, M. A.; Datla, R.; Sikka, V.; Jones, A.; Choi, C.-H. Experimental Study of Skin Friction Drag Reduction on Superhydrophobic Flat Plates in High Reynolds Number Boundary Layer Flow. *Phys. Fluids* **2013**, *25*, 025103.
(11) Smith, J. D.; Dhiman, R.; Anand, S.; Reza-Garduno, E.; Cohen, R. E.; McKinley, G. H.; Varanasi, K. K. Droplet Mobility on Lubricant-Impregnated Surfaces. *Soft Matter* **2013**, *9*, 1772−1780.
(12) Leslie, D. C.; Waterhouse, A.; Berthet, J. B.; Valentin, T. M.; Watters, A. L.; Jain, A.; Kim, P.; Hatton, B. D.; Nedder, A.; Donovan, K.; Super, E. H.; Howell, C.; Johnson, C. P.; Vu, T. L.; Bolgen, D. E.; Rifai, S.; Hansen, A. R.; Aizenberg, M.; Super, M.; Aizenberg, J.; Ingber, D. E. A Bioinspired Omniphobic Surface Coating on Medical Devices Prevents Thrombosis and Biofouling. *Nat. Biotechnol.* **2014**, *32*, 1134−1140.
(13) Choi, C.-H.; Hagvall, S. H.; Wu, B. M.; Dunn, J. C. Y.; Beygui, R. E.; Kim, C.-J. Cell Interaction with Three-Dimensional Sharp-Tip Nanotopography. *Biomaterials* **2007**, *28*, 1672−1679.
(14) Choi, C.-H.; Heydarkhan-Hagvall, S.; Wu, B. M.; Dunn, J. C. Y.; Beygui, R. E.; Kim, C.-J. Cell Growth as a Sheet on Three-Dimensional Sharp-Tip Nanostructures. *J. Biomed. Mater. Res., Part A* **2009**, *89A*, 804−817.
(15) Guo, P.; Zheng, Y.; Wen, M.; Song, C.; Lin, Y.; Jiang, L. Icephobic/Anti-Icing Properties of Micro/Nanostructured Surfaces. *Adv. Mater.* **2012**, *24*, 2642−2648.
(16) Sarshar, M. A.; Swarctz, C.; Hunter, S.; Simpson, J.; Choi, C. H. Effects of Contact Angle Hysteresis on Ice Adhesion and Growth on Superhydrophobic Surfaces under Dynamic Flow Conditions. *Colloid Polym. Sci.* **2013**, *291*, 427−435.
(17) Varanasi, K. K.; Deng, T.; Smith, J. D.; Hsu, M.; Bhate, N. Frost Formation and Ice Adhesion on Superhydrophobic Surfaces. *Appl. Phys. Lett.* **2010**, *97*, 234102.
(18) Xu, W.; Choi, C.-H. From Sticky to Slippery Droplets: Dynamics of Contact Line Depinning on Superhydrophobic Surfaces. *Phys. Rev. Lett.* **2012**, *109*, 024504.
(19) Liu, M.; Zheng, Y.; Zhai, J.; Jiang, L. Bioinspired Super-Antiwetting Interfaces with Special Liquid-Solid Adhesion. *Acc. Chem. Res.* **2010**, *43*, 368−377.
(20) Krupenkin, T. N.; Taylor, J. A.; Wang, E. N.; Kolodner, P.; Hodes, M.; Salamon, T. R. Reversible Wetting-Dewetting Transitions on Electrically Tunable Superhydrophobic Nanostructured Surfaces. *Langmuir* **2007**, *23*, 9128−9133.
(21) Chen, X.; Ma, R.; Li, J.; Hao, C.; Guo, W.; Luk, B. L.; Li, S. C.; Yao, S.; Wang, Z. Evaporation of Droplets on Superhydrophobic Surfaces: Surface Roughness and Small Droplet Size Effects. *Phys. Rev. Lett.* **2012**, *109*, 116101.
(22) Yuan, J.; Liu, X.; Akbulut, O.; Hu, J.; Suib, S. L.; Kong, J.; Stellacci, F. Superwetting Nanowire Membranes for Selective Absorption. *Nat. Nanotechnol.* **2008**, *3*, 332−336.
(23) Liu, X.; Ye, Q.; Yu, B.; Liang, Y.; Liu, W.; Zhou, F. Switching Water Droplet Adhesion Using Responsive Polymer Brushes. *Langmuir* **2010**, *26*, 12377−12382.
(24) Zhao, X.; Fan, H.; Luo, J.; Ding, J.; Liu, X.; Zou, B.; Feng, Y. Electrically Adjustable, Super Adhesive Force of a Superhydrophobic Aligned Mno2 Nanotube Membrane. *Adv. Funct. Mater.* **2011**, *21*, 184−190.
(25) Yao, X.; Gao, J.; Song, Y.; Jiang, L. Superoleophobic Surfaces with Controllable Oil Adhesion and Their Application in Oil Transportation. *Adv. Funct. Mater.* **2011**, *21*, 4270−4276.
(26) Xia, F.; Jiang, L. Bio-Inspired, Smart, Multiscale Interfacial Materials. *Adv. Mater.* **2008**, *20*, 2842−2858.
(27) Liu, M.; Jiang, L. Switchable Adhesion on Liquid/Solid Interfaces. *Adv. Funct. Mater.* **2010**, *20*, 3753−3764.
(28) Zhang, L.; Zhang, Z.; Wang, P. Smart Surfaces with Switchable Superoleophilicity and Superoleophobicity in Aqueous Media: Toward Controllable Oil/Water Separation. *NPG Asia Mater.* **2012**, *4*, e8.
(29) Feng, X.; Feng, L.; Jin, M.; Zhai, J.; Jiang, L.; Zhu, D. Reversible Super-Hydrophobicity to Super-Hydrophilicity Transition of Aligned ZnO Nanorod Films. *J. Am. Chem. Soc.* **2004**, *126*, 62−63.
(30) Li, C.; Guo, R.; Jiang, X.; Hu, S.; Li, L.; Cao, X.; Yang, H.; Song, Y.; Ma, Y.; Jiang, L. Reversible Switching of Water-Droplet Mobility on a Superhydrophobic Surface Based on a Phase Transition of a Side-Chain Liquid-Crystal Polymer. *Adv. Mater.* **2009**, *21*, 4254−4258.
(31) Krupenkin, T. N.; Taylor, J. A.; Schneider, T. M.; Yang, S. From Rolling Ball to Complete Wetting: The Dynamic Tuning of Liquids on Nanostructured Surfaces. *Langmuir* **2004**, *20*, 3824−3827.
(32) Cheng, Z.; Feng, L.; Jiang, L. Tunable Adhesive Superhydrophobic Surfaces for Superparamagnetic Microdroplets. *Adv. Funct. Mater.* **2008**, *18*, 3219−3225.
(33) Wu, D.; Wu, S.-Z.; Chen, Q.-D.; Zhang, Y.-L.; Yao, J.; Yao, X.; Niu, L.-G.; Wang, J.-N.; Jiang, L.; Sun, H.-B. Curvature-Driven Reversible *in situ* Switching between Pinned and Roll_Down Superhydrophobic States for Water Droplet Transportation. *Adv. Mater.* **2011**, *23*, 545−549.
(34) Lu, Y.; Sarshar, M. A.; Du, K.; Chou, T.; Choi, C.-H.; Sukhishvili, S. A. Large-Amplitude, Reversible, pH-Triggered Wetting Transitions Enabled by Layer-by-Layer Films. *ACS Appl. Mater. Interfaces* **2013**, *5*, 12617−12623.
(35) Waghmare, P. R.; Das, S.; Mitra, S. K. Under-Water Superoleophobic Glass: Unexplored Role of the Surfactant-Rich Solvent. *Sci. Rep.* **2013**, *3*, 1862.
(36) Miwa, M.; Nakajima, A.; Fujishima, A.; Hashimoto, K.; Watanabe, T. Effects of the Surface Roughness on Sliding Angles of Water Droplets on Superhydrophobic Surfaces. *Langmuir* **2000**, *16*, 5754−5760.
(37) Tsai, Y.-T.; Choi, C.-H.; Gao, N.; Yang, E.-H. Tunable Wetting Mechanism of Polypyrrole Surfaces and Low-Voltage Droplet Manipulation via Redox. *Langmuir* **2011**, *27*, 4249−4256.
(38) Pei, Q.; Inganaes, O. Electrochemical Applications of the Bending Beam Method. 2. Electroshrinking and Slow Relaxation in Polypyrrole. *J. Phys. Chem.* **1993**, *97*, 6034−6041.
(39) Matencio, T.; De Paoli, M. A.; Peres, R. C. D.; Torresi, R. M.; Cordoba de Torresi, S. I. Ionic Exchanges in Dodecylbenzenesulfonate Doped Polypyrrole Part 1. Optical Beam Deflection Studies. *Synth. Met.* **1995**, *72*, 59−64.
(40) Matencio, T.; De Paoli, M. A.; Peres, R. C. D.; Torresi, R.; Cordoba de Torresi, S. I. Ionic Diffusion Processes in Polypyrrole. *J. Braz. Chem. Soc.* **1994**, *5* (3), 191−196.
(41) Stauffer, C. E. The Measurement of Surface Tension by the Pendant Drop Technique. *J. Phys. Chem.* **1965**, *69*, 1933−1938.
(42) Roe, R. J.; Bacchetta, V. L.; Wong, P. M. G. Refinement of Pendent Drop Method for the Measurement of Surface Tension of Viscous Liquid. *J. Phys. Chem.* **1967**, *71*, 4190−4193.
(43) Berthier, J. *Microdrops and Digital Microfluidics*; William Andrew Inc.: Norwick, NY, 2008.
(44) Liu, M.; Liu, X.; Ding, C.; Wei, Z.; Zhu, Y.; Jiang, L. Reversible Underwater Switching between Superoleophobicity and Superoleophilicity on Conducting Polymer Nanotube Arrays. *Soft Matter* **2011**, *7*, 4163−4165.
(45) Halldorsson, J. A.; Little, S. J.; Diamond, D.; Spinks, G.; Wallace, G. Controlled Transport of Droplets Using Conducting Polymers. *Langmuir* **2009**, *25*, 11137−11141.
(46) Halldorsson, J. A.; Wu, Y.; Brown, H. R.; Spinks, G. M.; Wallace, G. G. Surfactant-Controlled Shape Change of Organic Droplets Using Polypyrrole. *Thin Solid Films* **2011**, *519*, 6486−6491.
(47) Wang, X.; Smela, E. Color and Volume Change in PPy(DBS). *J. Phys. Chem. C* **2009**, *113*, 359−368.
(48) Teh, K. S.; Takahashi, Y.; Yao, Z.; Lu, Y.-W. Influence of Redox-Induced Restructuring of Polypyrrole on Its Surface Morphology and Wettability. *Sens. Actuators, A* **2009**, *155*, 113−119.
(49) Liu, M.; Nie, F.-Q.; Wei, Z.; Song, Y.; Jiang, L. *In Situ* Electrochemical Switching of Wetting State of Oil Droplet on Conducting Polymer Films. *Langmuir* **2010**, *26*, 3993−3997.
(50) Bay, L.; Jacobsen, T.; Skaarup, S.; West, K. Mechanism of Actuation in Conducting Polymers: Osmotic Expansion. *J. Phys. Chem. B* **2001**, *105*, 8492−8497.

DOI: 10.1021/acsami.5b07589
ACS Appl. Mater. Interfaces XXXX, XXX, XXX−XXX

(51) Lai, Y.; Lin, C.; Huang, J.; Zhuang, H.; Sun, L.; Nguyen, T. Markedly Controllable Adhesion of Superhydrophobic Spongelike Nanostructure TiO_2 Films. *Langmuir* **2008**, *24*, 3867−3873.
(52) Di Mundo, R.; Palumbo, F.; d'Agostino, R. Nanotexturing of Polystyrene Surface in Fluorocarbon Plasmas: From Sticky to Slippery Superhydrophobicity. *Langmuir* **2008**, *24*, 5044−5051.

DOI: 10.1021/acsami.5b07589
ACS Appl. Mater. Interfaces XXXX, XXX, XXX−XXX